Parameter Estimation of Large Scale Systems using Dynamic Data Monitoring: Application to Plume Dispersion Phenomenon

R. Madankan, P. Singla

Mechanical and Aerospace Engineering Department, University at Buffalo, Buffalo, NY,14228

Abstract. In this research, the effects of data measurement on source parameter estimation are studied. The concept of mutual information is applied to locate the optimal location for each sensor to improve the accuracy of the overall estimation process. For validation purposes, an advection - diffusion simulation code, SCIPUFF (Second-order Closure Integrated PUFF) is used as a modeling testbed to study the effects of using dynamic data measurement. Bayesian inference framework is utilized to perform source parameter estimation using stationary and mobile sensor networks, where in mobile sensors, the proposed approach of Dynamic Data Monitoring is used to locate mobile data observation sensors. As our numerical simulations show, using dynamic data monitoring leads to a *considerably* better estimate of the source parameters, while just using fewer sensors, than the stationary sensors case, or other alternative approaches.

1 Introduction

Emission of toxic material clouds from sources, such as industrial plants, vehicular traffic, deliberate toxic releases, and volcanic eruptions is one of the potential threats to environment and human society. With increasing number of instances of toxic material release, there is tremendous interest in precise source characterization and generating accurate hazard maps of toxic material dispersion for appropriate disaster management. Different types of algorithms have been proposed to characterize source parameters in plume dispersion phenomenon. Most of these algorithms can be divided into two major categories: optimization based methods and probabilistic methods. A comprehensive review about optimization and probabilistic based methods for source characterization in plume dispersion phenomenon, is performed by Zheng *et al.* [1] and Rao [2].

There is no doubt that proper sensor placement is intimately tied to the performance of the source estimation and model uncertainty characterization. Poor data measurements caused by sparse or scattered sensors over the domain of interest results in a poor estimate of source location. Hence finding optimal location of the sensor is very important for source parameter estimation. Due to dynamics of the plume dispersion phenomenon, it is much more efficient to

apply mobile sensors, instead of static sensors for data monitoring purposes. Different strategies have been suggested to determine the optimal path of the mobile sensors for source parameters characterization. Earlier works in this area can be categorized as Chemotaxis [3], Anemotaxis [4], and Fluxotaxis [5].

In chemotaxis approach [3], mobile sensors follow the concentration gradient. Therefore, the direction of the largest concentration is the goal direction for the chemotaxis. In anemotaxis strategy [4], mobile sensors always move upstream while they locate inside the plume, hence the upstream is the goal direction for mobile sensors. With fluxotaxis approach [5], the mobile sensors compute the amount of dispersal material flux passing through virtual surfaces formed by neighboring sensors. Where, each individual sensor independently calculates the amount of local material flux, relative to the current position of its neighbors.

Even though, each of above approaches has its own advantage and application, but the major drawback of aforementioned approaches lies in the possibility of being trapped in local maxima and plateaus of the concentration field.

Besides aforementioned methods, recently multiple researches have been done on the field of optimal sensor placement, based on information theory. Choi *et al.* [6] studied continuous motion planning of mobile sensors for Informative forecasting in presence of *linear time varying* systems and Gaussian uncertainty. Bourgault *et al.* [7] suggested a robotic exploration approach based on maximizing mutual information, while linearizing the dynamics and sensor model and assuming *Gaussian* uncertainty involved in the process.

Optimal sensor placement is also widely used in target tracking problem [8,9,10]. For instance, MartiNez *et al.* [9] applied optimal sensor placement and motion coordination of mobile sensor networks to tackle target tracking problem. This is achieved by maximizing the Fisher Information matrix, or equivalently minimizing the associated Cramer-Rao lower bound of parameter estimates. Tharmarasa *et al.* [10] studied the problem of selecting a small subset of the available sensors in a large network of sensors in order to track multiple targets. A search scheme based on combination of optimization methods and Cramer-Rao lower bound was used to perform this task. The major drawback of these works is that Fisher Information matrix usually consists of the parameter which is to be estimated. Hence, an estimate of unknown parameters is used during maximization of Fisher Information matrix. Williams *et al.* [11] studied the problem of choosing optimal subset of sensors from a *stationary* sensor network, in presence of *linear* model dynamics and *linear* sensor model, while minimizing communication cost. The major drawback of this work is that it doesn't consider any dynamic for applied sensors. Hence, a large *stationary* sensor network is needed (while a small portion of them is used at each time) to assure the performance of proposed approach. As well, linearity assumptions in dynamic model and sensor model restrict applicability of this method. In a research by Julian *et al.* [8], an information theoretic framework was presented for distributive control of a set of mobile robots. The basic idea of this work is to move applied mobile robots along gradient of mutual information to maximize information collection. The major drawback of this approach is that it may not be effective

in the case that initial positions of robots are far way from regions of interest (local optimality). Also, importance sampling techniques were used to calculate gradient of mutual information, which could result in computational delay. Hoffmann *et al.* [12] presented a control approach for mobile sensor networks, based on maximizing mutual information. In detail, he used a particle filter framework and Monte Carlo integration method for evaluation of mutual information. Also, an iterative approach was used at each time step to find optimal control signal for each mobile sensor. The major benefit of proposed approach is that applied particle filter framework makes it possible to directly use the proposed method in presence of possible non-Gaussian uncertainty and nonlinear dynamic and/or observation models. However, using Monte Carlo integration while evaluating mutual information can reduce its computational performance. Another drawback in proposed method is that proposed control approach should be solved at each time step iteratively, which could result in computational cost.

The key idea of this paper is to *optimally* allocate data monitoring sensors over the spatial domain of interest such that the uncertainty involved in source parameter estimates is minimized. This has been achieved by maximizing the mutual information between the model output and data measurements. A dynamic programming based approach is used to maximize the mutual information between uncertain parameters and observational data. As it will be shown, proposed approach expedites the convergence of estimation process and avoids possible local optimalities while finding mobile sensor locations by maximizing the mutual information, rather moving along its gradient. In other words, proposed approach moves the mobile sensors toward the plume, even though the sensors are initially located far from the plume area. Along proposed approach for optimal sensor placement, a combination of generalized Polynomial Chaos (gPC) and Bayesian inference is used for data assimilation process which allows us to apply our method in presence of nonlinear dynamics and sensor model and non-Gaussian uncertainties, without using any Monte Carlo sampling. As well, a set of recently developed quadrature points, named as Conjugate Unscented Transform points [13,14,15,16], are used to alleviate the computational complexities associated with evaluation of mutual information, uncertainty propagation, and estimation process.

Outline of this article is as follows: first, mathematical description of the problem is presented in section 2 and overall perspective of the proposed methodology for estimation process is described in section 3. In section 4, proposed mathematical framework for uncertainty quantification is presented. Next, applied data assimilation approach for parameter estimation is briefly described in section 5. Mathematical details of the dynamic data monitoring for optimal sensor placement is explained in section 6. Numerical simulations are then presented in section 7 to demonstrate the performance of the proposed approach. Finally, conclusion is presented in section 8.

2 Problem Statement

The plume dispersion phenomenon can be modeled as the following discrete model:

$$\mathbf{x}_{k+1}(\boldsymbol{\Theta}) = f(\mathbf{x}_k, \boldsymbol{\Theta}) \tag{1}$$

where, $\mathbf{x}_k \in \mathbb{R}^n$ denotes concentration of pollutant material at time step t_k and $\boldsymbol{\Theta} \in \mathbb{R}^m$ represents source parameters of dynamical model that are assumed to be uncertain with a given prior probability $p(\boldsymbol{\Theta})$. Note that in Eq. (1) the concentration $\mathbf{x}_k$ is a function of spatial position (lat, lon, z), i.e. $\mathbf{x}_k(\boldsymbol{\Theta}) \equiv \mathbf{x}_k(lat, lon, z, \boldsymbol{\Theta})$.

In addition, assume that some observation of concentration $\mathbf{x}_k$ is available at some specific spatial locations over the domain, i.e.

$$\mathbf{z}_k(\boldsymbol{\Theta}, \mathbf{x}_k) = h(\mathbf{x}_k, \boldsymbol{\Theta}, \nu_k) \tag{2}$$

where, $\mathbf{z}_k \in \mathbb{R}^b$ is the observation vector at time step t_k and $h(.)$ is the observation operator which can be nonlinear. True value of concentration $\mathbf{x}_k$ is polluted with some noise ν_k. Note that dimension of observation vector is generally much smaller than the dimension of $\mathbf{x}_k$, i.e. $b \ll n$. Also, like concentration $\mathbf{x}_k$, observation $\mathbf{z}_k$ is a function of spatial position (lat, lon, z), i.e. $\mathbf{z}_k(\boldsymbol{\Theta}) \equiv \mathbf{z}_k(lat, lon, z, \boldsymbol{\Theta})$

Our final goal is to precisely estimate source parameter $\boldsymbol{\Theta}$, given some observations of concentration. The performance of this estimation process crucially depends on the spatial position of observations in hand. In other words, using observations from different spatial locations can result in different estimates for source parameters $\boldsymbol{\Theta}$. Hence, the primary focus of this paper is to develop a mathematical framework to find the *optimal* locations of sensors for making efficient observations so as to enhance the data assimilation process.

3 Methodology

Proposed approach in this paper consists of three different components that are combined together to perform the task of source parameter estimation. These components consist of i) Uncertainty Quantification (UQ), ii) Dynamic Data Monitoring (DDM), and iii) Data Assimilation (DA). Schematic view of whole estimation process is shown in Fig. 1. As shown in Fig. 1, estimation process starts with a given uncertainty in source parameters of a dispersion phenomenon. The first step to perform the estimation is to quantify the effect of uncertain source parameters on spatial-temporal distribution of concentration of dispersive material. This is performed by propagation of a set of quadrature points through the numerical model. Weighted average of propagated quadrature points are then used to determine *prior* statistics of dispersive material (e.g. mean and covariance) over the spatial domain at a given time. Precise approximation of prior statistics is crucial to ensure the performance of estimation process. Hence, utilizing an *appropriate* and *efficient* set of quadrature points is of high importance. In section 4, the methodology for UQ is discussed in further detail .

Besides precise quantification of uncertainty, having *useful* measurement data is also highly important to ensure accurate source parameter estimation. DDM is utilized to perform this task during the estimation process. The key goal of DDM is to optimally allocate a set of mobile sensors (Unmanned Aerial Vehicles) such that measurement of *better data* is guarantied at each time step. This is achieved by maximizing the mutual information between model predictions and observed data, given a set of kinetic constraints on mobile sensors. Dynamic programming [17][18] is used to solve this optimization problem. This will result in a set of control signals that are applied to each mobile sensor at each time step t_k and determine the optimal locations for data monitoring sensors. Detailed explanations about DDM are presented in section 6.

Finally, obtained prior statistics from UQ and observed data from DDM are combined together in a Bayesian inference framework to complete the estimation process. This results in *posterior* value for statistics of source parameters estimates. These posterior statistics are then used to approximate posterior distribution of source parameters by using a polynomial chaos methodology. Detailed information about DA is presented in section 5.

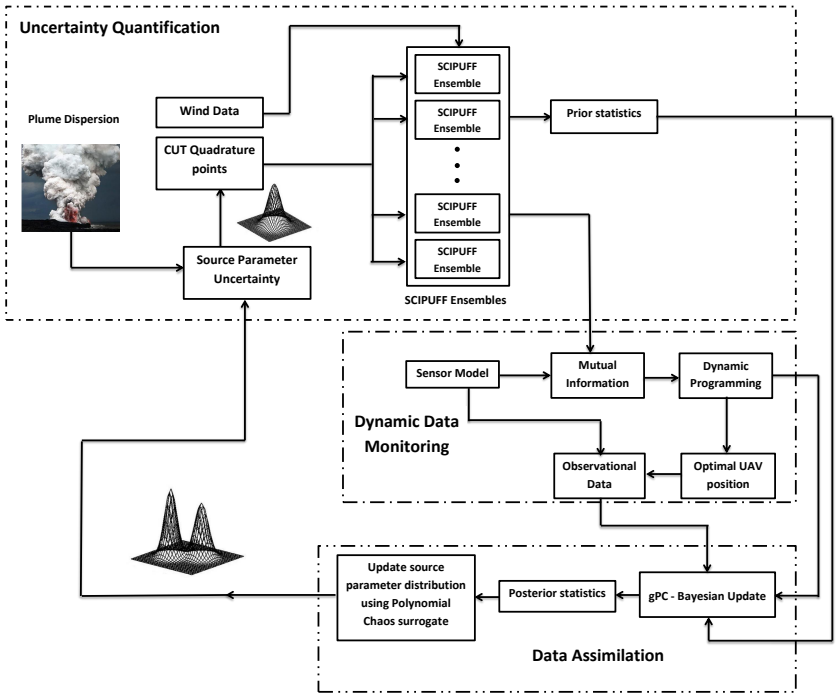

Fig. 1. Schematic view of the source parameter estimation process

4 Uncertainty Quantification

Method of quadrature points is utilized to perform the task of uncertainty quantification. In this method, a set of *intelligently* selected points will be propagated through the dynamical model and statistics of the output are then determined by weighted average of model outputs. In fact, method of quadrature points can be viewed as a MC-like evaluation of system of equations, but with sample points selected by quadrature rules.

To explain this in more detail, let $\mathbf{x}(lat, lon, z, \boldsymbol{\Theta}, t) \in \mathbb{R}^n$ represent the concentration of pollutant material at a given spatial point (lat, lon, z) and time t. Note that $\mathbf{x}$ is a function of uncertain model parameter vector $\boldsymbol{\Theta} = [\boldsymbol{\theta}_1, \boldsymbol{\theta}_2, \cdots, \boldsymbol{\theta}_m]^T \in \mathbb{R}^m$. The parameter vector $\boldsymbol{\Theta}$ contains source parameters like source location, total mass of pollutant material, etc. $\boldsymbol{\Theta}$ is assumed to be time invariant and function of a random vector $\boldsymbol{\xi} = [\xi_1, \xi_2, \cdots, \xi_m]^T \in \mathbb{R}^m$ defined by a pdf $p(\boldsymbol{\xi})$ over the support Ω.

Now, k^{th} order moment of model output $\mathbf{x}$, at a given point (lat, lon, z) on the domain and a specific time t can be written as

$$\mathcal{E}[\mathbf{x}^k(lat, lon, z, \boldsymbol{\Theta}, t)] = \int_{\boldsymbol{\xi}} \mathbf{x}^k(lat, lon, z, \boldsymbol{\Theta}, t) p(\boldsymbol{\xi}) d\boldsymbol{\xi} \simeq \sum_{q}^{M} w_q \mathbf{x}^k(lat, lon, z, \boldsymbol{\Theta}(\boldsymbol{\xi}^q), t), \quad k = 1, 2, \cdots \tag{3}$$

where, M denotes total number of applied quadrature points and $\boldsymbol{\Theta}(\boldsymbol{\xi}^q) \in \mathbb{R}^{m \times 1}$ represents q^{th} quadrature point, generated based on applied quadrature scheme. Similarly, k^{th} order central moments of concentration at each point (lat, lon, z) can be evaluated by shifting the quadrature points by the computed mean and then using Eq. (3).

Different types of quadrature rules like classical Gaussian quadrature rule can be used to evaluate the integral in Eq. (3). The classic method of Gaussian quadrature exactly integrates polynomials of 1-Dimension up to degree $2M + 1$ with $M + 1$ quadrature points. Generally, in an n-dimensional parameter space, the tensor product of 1-dimension quadrature points is used to generate quadrature points. As a consequence of this, the number of quadrature points increases exponentially as the number of input parameters increases. Hence, using more efficient quadrature schemes, which doesn't exponentially

Herein, we have utilized Conjugate Unscented Transform (CUT) recently developed by Nagavenkat *et al.* [14,15,16], to overcome this drawback of regular quadrature points. CUT points are efficient in terms of accuracy while integrating polynomials and yet just employ a small fraction of the number of points used by the traditional Gaussian quadrature scheme. Fig. 2 represents the number of 8^{th} order quadrature points required by different quadrature schemes (CUT, Gauss-Legendre, Clenshaw-Curtis and Sparse Grid) for a uniformly distributed random vector versus the dimensionality of the random vector. From this figure, it is clear that the growth of number of quadrature points with increase in

dimensionality according to the CUT methodology is much lower as compared to the Gauss-Legendre and Clenshaw-Curtis. Furthermore, it is apparent that the CUT methodology requires less than one half of quadrature points as required by the sparse grid Smolyak approach. For example, 59 CUT quadrature points are required to satisfy 8^{th} order moments in 3-dimensional space as compared to 165 Sparse Grid quadrature points, 125 Gauss-Legendre quadrature points and 729 Clenshaw-Curtis quadrature points. Hence, the CUT methodology can be very useful in reducing the number of numerical model runs which needs to be performed for accurate computation of prior statistics.

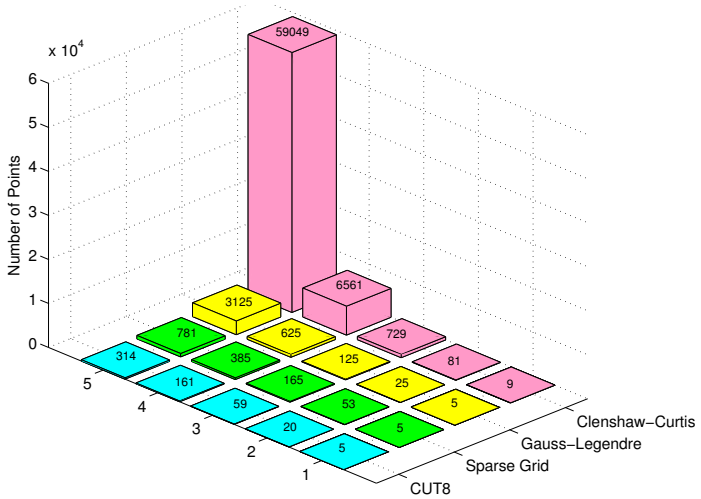

Fig. 2. Comparison of number of 8^{th} order quadrature points required according to different quadrature scheme versus dimension of random variable.

5 Data Assimilation

The purpose of data assimilation is to fuse the information provided by the model forecasts and sensor observations to correct and refine the distribution of the source parameters and to improve our level of confidence about the uncertain parameters.

This problem can be described as finding the posterior statistics of the parameter vector $\boldsymbol{\Theta} = [\boldsymbol{\theta}_1, \boldsymbol{\theta}_2, \cdots, \boldsymbol{\theta}_m]^T \in \mathbb{R}^m$, given a set of measurement data $\mathcal{Z} = \{\mathbf{z}^1, \mathbf{z}^2, \cdots, \mathbf{z}^N\}$, where N denotes the total number of time steps where measurement data is available. Using Bayes' theorem, posterior distribution of $\boldsymbol{\Theta}$ can be written as:

$$p(\boldsymbol{\Theta}|\mathcal{Z}) = \frac{p(\boldsymbol{\Theta})p(\mathcal{Z}|\boldsymbol{\Theta})}{p(\mathcal{Z})} \tag{4}$$

where, $p(\boldsymbol{\Theta})$ is the prior distribution of parameter $\boldsymbol{\Theta}$, $p(\mathcal{Z}|\boldsymbol{\Theta})$ is the likelihood of measurements given the parameter, and $p(\mathcal{Z})$ is the probability density function of measurements $\mathcal{Z}$, which is equal to:

$$p(\mathcal{Z}) = \int_{\boldsymbol{\Theta}} p(\mathcal{Z}|\boldsymbol{\Theta})p(\boldsymbol{\Theta})d\boldsymbol{\Theta} = \mathcal{E}_{\boldsymbol{\Theta}}\{p(\mathcal{Z}|\boldsymbol{\Theta})\} \tag{5}$$

Now, one can compute the posterior statistics of $\boldsymbol{\Theta}$ by multiplication of appropriate functions of $\boldsymbol{\Theta}$ in Eq. (4) and integrating with respect to $\boldsymbol{\Theta}$ [19]. For instance, posterior mean of $\boldsymbol{\Theta}$, denoted by $\hat{\boldsymbol{\Theta}}^{+}$, can be computed as:

$$\hat{\boldsymbol{\Theta}}^{+} = \mathcal{E}_{\boldsymbol{\Theta}}\{\boldsymbol{\Theta}\} = \frac{\int_{\boldsymbol{\Theta}} \boldsymbol{\Theta} p(\boldsymbol{\Theta})p(\mathcal{Z}|\boldsymbol{\Theta})d\boldsymbol{\Theta}}{\mathcal{E}_{\boldsymbol{\Theta}}\{p(\mathcal{Z}|\boldsymbol{\Theta})\}} = \frac{\mathcal{E}_{\boldsymbol{\Theta}}\{\boldsymbol{\Theta} p(\mathcal{Z}|\boldsymbol{\Theta})\}}{\mathcal{E}_{\boldsymbol{\Theta}}\{p(\mathcal{Z}|\boldsymbol{\Theta})\}} \tag{6}$$

Posterior second order moment of $\boldsymbol{\Theta}$, denoted by Σ^{+}, can also be computed as:

$$\Sigma^{+} = \int_{\boldsymbol{\Theta}} \boldsymbol{\Theta}\boldsymbol{\Theta}^{T} p(\boldsymbol{\Theta}|\mathcal{Z})d\boldsymbol{\Theta} = \frac{\mathcal{E}_{\boldsymbol{\Theta}}\{\boldsymbol{\Theta}\boldsymbol{\Theta}^{T} p(\mathcal{Z}|\boldsymbol{\Theta})\}}{\mathcal{E}_{\boldsymbol{\Theta}}\{p(\mathcal{Z}|\boldsymbol{\Theta})\}} \tag{7}$$

Note that CUT quadrature points are used to evaluate the expected values in Eq. (6) and Eq. (7). i.e.

$$\mathcal{E}_{\boldsymbol{\Theta}}\{\boldsymbol{\Theta} p(\mathcal{Z}|\boldsymbol{\Theta})\} \simeq \sum_{q=1}^{N_q} w_q \boldsymbol{\Theta}(\boldsymbol{\xi}^q) p(\mathcal{Z}|\boldsymbol{\Theta}(\boldsymbol{\xi}^q)) \tag{8}$$

$$\mathcal{E}_{\boldsymbol{\Theta}}\{\boldsymbol{\Theta}\boldsymbol{\Theta}^{T} p(\mathcal{Z}|\boldsymbol{\Theta})\} \simeq \sum_{q=1}^{N_q} w_q \boldsymbol{\Theta}(\boldsymbol{\xi}^q)\boldsymbol{\Theta}^{T}(\boldsymbol{\xi}^q) p(\mathcal{Z}|\boldsymbol{\Theta}(\boldsymbol{\xi}^q)) \tag{9}$$

$$\mathcal{E}_{\boldsymbol{\Theta}}\{p(\mathcal{Z}|\boldsymbol{\Theta})\} \simeq \sum_{q=1}^{N_q} w_q p(\mathcal{Z}|\boldsymbol{\Theta}(\boldsymbol{\xi}^q)) \tag{10}$$

where, $\boldsymbol{\Theta}(\boldsymbol{\xi}^q)$ represents the q^{th} quadrature value of the parameter vector $\boldsymbol{\Theta}$, generated according to $p(\boldsymbol{\Theta})$., and w_q is the corresponding weight of quadrature point $\boldsymbol{\Theta}(\boldsymbol{\xi}^q)$.

5.1 Computation of Posterior Probability of Source Parameters

The posterior statistics obtained from Bayesian update can be used to approximate the posterior distribution of parameter $\boldsymbol{\Theta}$. This can be achieved by making use of Generalized Polynomial Chaos (gPC) Theory [20,21].

Based on the gPC theory, uncertain system parameter $\boldsymbol{\Theta}$ can be approximated as a linear combination of basis functions, $\phi_k(\boldsymbol{\xi})$, which span the stochastic space of random variables $\boldsymbol{\xi} = [\boldsymbol{\xi}_1, \cdots \boldsymbol{\xi}_m]^T$:

$$\theta_i(\boldsymbol{\xi}) = \sum_{k=0}^{L} \theta_{i_k} \phi_k(\boldsymbol{\xi}) \tag{11}$$

The coefficients θ_{i_k} are obtained by making use of the following *normal equation*:

$$\theta_{i_k} = \frac{\mathcal{E}[\theta_i(\boldsymbol{\xi})\phi_k(\boldsymbol{\xi})]}{\mathcal{E}[\phi_k(\boldsymbol{\xi})\phi_k(\boldsymbol{\xi})]} \tag{12}$$

Note that the integrals involved in Eq. (12) can be evaluated using quadrature scheme.

$$\mathcal{E}[\phi_k(\boldsymbol{\xi}), \phi_k(\boldsymbol{\xi})] \simeq \sum_{q=1}^{M} w_q \phi_k^2(\boldsymbol{\xi}_q) \tag{13}$$

$$\mathcal{E}[\theta_i(\boldsymbol{\xi}), \phi_k(\boldsymbol{\xi})] \simeq \sum_{q=1}^{M} w_q \theta_i(\boldsymbol{\xi}_q)\phi_k(\boldsymbol{\xi}_q) \tag{14}$$

Given posterior statistics of parameter $\boldsymbol{\Theta}$, one can update the polynomial expansion coefficients of Eq. (11) as described in [19]. This results in a set of nonlinear algebraic equations which can be solved to find posterior coefficients of gPC expansion of $\boldsymbol{\Theta}$:

$$\theta_{i_1}^{+} = \hat{\boldsymbol{\Theta}}_i^{+}, \quad i = 1, 2, \cdots, m \tag{15}$$

$$\sum_{k=0}^{L} \boldsymbol{\theta}_{i_k}^{+} \boldsymbol{\theta}_{j_k}^{+} = \boldsymbol{\Sigma}^{+}(i, j), \quad i, j = 1, \cdots, m \tag{16}$$

Notice that Eq. (15) directly results in values of $\boldsymbol{\Theta}_{pc_1}^{+}$ components, while Eq. (16) provides m^2 equations for remaining mL unknown coefficients. Depending on order of applied PC expansion and dimension of $\boldsymbol{\Theta}$, obtained set of equations can be over determined, determined, or under determined. Different approaches like nonlinear least square method can be used to solve Eq. (16) in case of over determined set of equations, while for under determined set of equations, regularization techniques can be used to find a solution for the posterior coefficients of polynomial expansion.

6 Dynamic Data Monitoring: Methodology

The major role of DDM module is to *optimally* locate a set of mobile sensors such that measurements with *more information content* are sought at each time step. Optimal location of each mobile sensor at each time step can be achieved by maximizing the *mutual information* between model predictions and observed data. In the following, we first explain the concept of mutual information and applied mobile sensor models. Then the mathematical details for optimal allocation of mobile sensors are presented.

Mutual Information as a measure for Sensor performance

According to information theory, the mutual information between source parameter $\boldsymbol{\Theta}$ and measurement $\mathbf{z}$ can be written as, [22],

$$I(\boldsymbol{\Theta};\mathbf{z}) = \int_{\mathbf{z}}\int_{\boldsymbol{\Theta}} p(\boldsymbol{\Theta},\mathbf{z}) \ln\left(\frac{p(\boldsymbol{\Theta},\mathbf{z})}{p(\boldsymbol{\Theta})p(\mathbf{z})}\right) d\boldsymbol{\Theta} d\mathbf{z} \tag{17}$$

Using Bayes' rule, $p(\boldsymbol{\Theta},\mathbf{z})$ can be written as

$$p(\boldsymbol{\Theta},\mathbf{z}) = p(\boldsymbol{\Theta}|\mathbf{z})p(\mathbf{z})$$

Hence $I(\boldsymbol{\Theta};\mathbf{z})$ will be equal to:

$$I(\boldsymbol{\Theta};\mathbf{z}) = \int_{\mathbf{z}} \underbrace{\int_{\boldsymbol{\Theta}} p(\boldsymbol{\Theta}|\mathbf{z}) ln\left(\frac{p(\boldsymbol{\Theta}|\mathbf{z})p(\mathbf{z})}{p(\boldsymbol{\Theta})p(\mathbf{z})}\right) d\boldsymbol{\Theta}}_{D_{KL}(p(\boldsymbol{\Theta}|\mathbf{z}))||p(\boldsymbol{\Theta})} p(\mathbf{z}) d\mathbf{z} \tag{18}$$

or,

$$I(\boldsymbol{\Theta};\mathbf{z}) = \mathcal{E}_z[D_{KL}\left(p(\boldsymbol{\Theta}|\mathbf{z})\right)||p(\boldsymbol{\Theta}))] \tag{19}$$

Hence, mutual information can be interpreted as the average Kullback-Leiber distance between prior pdf $p(\boldsymbol{\Theta})$ and posterior pdf $p(\boldsymbol{\Theta}|\mathbf{z})$. Hence, by maximizing mutual information one inherently maximizes the difference between prior and posterior distributions of parameter $\boldsymbol{\Theta}$, thus leading to a better measurement and estimate.

UAV model

We assume a set of Unmanned Aerial Vehicles (UAV) are used for data observation. Each of the UAVs is equipped with a chemical sensor to measure the concentration of pollutant material and the dynamic model of each of the UAVs is given as:

$$\mathbf{s}_{k+1}^v = F(\mathbf{s}_k^v, u_k^v), \quad v = 1, 2, \cdots, N_u \tag{20}$$

where N_u is total number of UAVs and k denotes k^{th} time step. Also, initial condition of v^{th} UAV is assumed to be given as $\mathbf{s}_0^v$. The state of UAV, $\mathbf{s}_k^v$, consists of (x, y, z) components of position and heading angle. The UAVs are modeled by the following discrete equations

$$\begin{bmatrix} s_1 \\ s_2 \\ \lambda \end{bmatrix}_{k+1} = \begin{bmatrix} s_1 \\ s_2 \\ \lambda \end{bmatrix}_k + \begin{bmatrix} u_k^{lon} \cos(\lambda_k + \frac{\pi u_k^\lambda}{2}) \\ u_k^{lat} \sin(\lambda_k + \frac{\pi u_k^\lambda}{2}) \\ \frac{\pi u_k^\lambda}{2} \end{bmatrix} \tag{21}$$

where $(s_1, s_2)_k$ is (lat, lon) coordinate of each UAV on spatial domain and λ_k represents heading angle of the UAV at time t_k. Control input of each UAV is composed of four different signals, i.e.

$$u_k = [u_k^{lon}, u_k^{lat}, u_k^\lambda]^T \tag{22}$$

In above equation, u_k^{lon} and u_k^{lat}, determine displacement of UAV in longitude and latitude directions, respectively; and u_k^λ determines heading angle for the

UAV. In here, we assumed that $u_k^{lat} = u_k^{lon} \equiv u_k^h$. Hence, our simplified model will be written as

$$\begin{bmatrix} s_1 \\ s_2 \\ \lambda \end{bmatrix}_{k+1} = \begin{bmatrix} s_1 \\ s_2 \\ \lambda \end{bmatrix}_k + \begin{bmatrix} u_k^h \cos(\lambda_k + \frac{\pi u_k^\lambda}{2}) \\ u_k^h \sin(\lambda_k + \frac{\pi u_k^\lambda}{2}) \\ \frac{\pi u_k^\lambda}{2} \end{bmatrix}, \qquad u_k = [u_k^h, u_k^\lambda]^T \tag{23}$$

It is assumed that u_k^λ takes one of the following discrete values:

$$u_k^\lambda = \begin{cases} -1, & \textit{move toward south} \\ 0, & \textit{move toward east} \\ 1, & \textit{move toward north} \\ 2, & \textit{move toward west} \\ 3, & s_{s+1} = s_k \end{cases} \tag{24}$$

As mentioned in Eq. (24), different values of u_k^λ determine the direction of the UAV at each time step t_k.

6.1 Optimal Sensor Placement

Our objective is to find a sequence of control inputs $U^{1:N_u} = \{u_0^{1:N_u}, u_1^{N_u}, \cdots, u_{N_t-1}^{1:N_u}\}$ such that it maximizes the mutual information between the sequence of expected observational data and the source parameters Θ over the time $t \in [t_1, t_{N_t}]$. This can be mathematically formulated as:

$$\max_{U^{1:N_u} = \{u_0^{1:N_u}, u_1^{1:N_u}, \cdots, u_{N_t-1}^{1:N_u}\}} J(\mathbf{s}_0^{1:N_u}) =$$

$$\max_{U^{1:N_u}} \sum_{v=1}^{N_u} I(\boldsymbol{\Theta}^1, \boldsymbol{\Theta}^2, \cdots, \boldsymbol{\Theta}^{N_t}; \mathbf{z}^1, \mathbf{z}^2, \cdots, \mathbf{z}^{N_t} | \mathbf{s}_1^{1:N_u}, \mathbf{s}_2^{1:N_u}, \cdots, \mathbf{s}_{N_t}^{1:N_u}) \tag{25}$$

constrained to

$$\begin{cases} \mathbf{s}_{k+1}^v = F(\mathbf{s}_k^v, u_k^v), \quad \mathbf{s}_0^v \qquad v = 1, 2, \cdots, N_u \\ s_k^a \neq \mathbf{s}_k^b, \quad a, b = 1, 2, \cdots, N_u, \quad a \neq b \end{cases} \tag{26}$$

where $\mathbf{z}^k$ and Θ^k are the measurement data and uncertain source parameter at time step t_k, respectively. N_t is the total number of time steps during the estimation process and Δ_t is the time interval between every two consecutive measurement updates. $\mathbf{s}_0^{1:N_u}$ represents initial conditions and $u_k^{1:N_u}$ denotes applied control signal at time t_k for a set of N_u UAVs. Note that in Eq. (25), it is assumed that measurement data from individual sensors or UAVs are independent.

As shown in Eq. (30), the optimization is constrained to the dynamic model for each UAV. Additionally, the second constraint in Eq. (30) is considered to avoid redundant observations at the same time instance.

Solving the above optimization problem requires finding optimal control signals for all the N_u UAVs over the time $t \in [t_1, t_{N_t}]$. Unfortunately, performing this optimization is computationally intractable. Hence, one needs to simplify the original problem and find the approximate solution for optimal control signals of each UAV.

One can use heuristic problem solving techniques like greedy algorithm [18] to simplify the aforementioned optimization problem. Using greedy algorithm, original optimization problem can be simplified to:

$$\max_{u_k^{1:N_u}} \; J(\mathbf{s}_0^{1:N_u}) = \max_{u_k^{1:N_u}} \sum_{v=1}^{N_u} I(\boldsymbol{\Theta}^k; \mathbf{z}^k | \mathbf{s}_k^v) \tag{27}$$

constrained to

$$\begin{cases} \mathbf{s}_k^v = F(\mathbf{s}_{k-1}^v, u_k^v), \quad \mathbf{s}_0^v \qquad v = 1, 2, \cdots, N_u \\ s_k^a \neq \mathbf{s}_k^b, \quad a, b = 1, 2, \cdots, N_u, \quad a \neq b \end{cases} \tag{28}$$

As one can see, Eq. (27) tries to maximize the mutual information at any given time step t_k. Hence, resulting in optimal control policy u_k for each of the UAVs.

Another alternative is to approximate the original optimization problem as the following:

$$\min_{U^{1:N_u} = \{u_0^{1:N_u}, u_1^{1:N_u}, \cdots, u_{N_t-1}^{1:N_u}\}} \; J(\mathbf{s}_0^{1:N_u}) = \max_{U^{1:N_u}} \sum_{v=1}^{N_u} I(\boldsymbol{\Theta}^1, \boldsymbol{\Theta}^2, \cdots, \boldsymbol{\Theta}^{N_t}; \mathbf{z}^1, \mathbf{z}^2, \cdots, \mathbf{z}^{N_t} | \mathbf{s}_1^v, \mathbf{s}_2^v, \cdots, \mathbf{s}_{N_t}^v) \simeq \min_{U^{1:N_u} = \{u_0^{1:N_u}, u_1^{1:N_u}, \cdots, u_{N_t-1}^{1:N_u}\}} \sum_{k=0}^{N_t-1} \left(\sum_{v=1}^{N_u} \left\{ -I(\boldsymbol{\Theta}^k; \mathbf{z}^k | \mathbf{s}_k^v) \right\} \right) \tag{29}$$

constrained to

$$\begin{cases} \mathbf{s}_{k+1}^v = F(\mathbf{s}_k^v, u_k^v), \quad \mathbf{s}_0^v \qquad v = 1, 2, \cdots, N_u \\ s_k^a \neq \mathbf{s}_k^b, \quad a, b = 1, 2, \cdots, N_u, \quad a \neq b \end{cases} \tag{30}$$

In above equations, $\mathbf{z}^k$ and Θ^k are the measurement data and uncertain source parameter at time step t_k, respectively. $I(\boldsymbol{\Theta}^k; \mathbf{z}^k | \mathbf{s}_k^v)$ represents the *Mutual Information* between the measurement data and source parameter, given v^{th} UAV position at time t_k. One should notice that Eq. (29) is a function of a sequence of control signals $U^{1:N_u} = \{u_0^{1:N_u}, u_1^{1:N_u}, \cdots, u_{N_t-1}^{1:N_u}\}$ which are enforced on a set of N_u UAVs during the time. Also, the cost function J is a function of initial position of UAVs, i.e. $J = J(\mathbf{s}_0^{1:N_u})$. Hence, the above optimization shall be performed for every possible combination for initial positions of N_u UAVs.

6.2 Dynamic Programming

Dynamic Programming [18] is used to find the optimal policy $U^{1:N_u}$ that minimizes Eq. (29). Optimal policy $U^{1:N_u} = \{u_0^{1:N_u}, u_1^{1:N_u}, \cdots, u_{N_t-1}^{1:N_u}\}$ is computed by backward optimization in time, i.e. first finding the optimal control input $u_{N_t-1}^{1:N_u}$, and then using $u_{N_t-1}^{1:N_u}$ to find optimal control signal $u_{N_t-2}^{1:N_u}$. This procedure will be repeated recursively to find the rest of the control signals u_k^vs. Generally, the following *recursive* algorithm [18] can be used to find optimal policy U^v that minimizes Eq. (29) for each UAV:

Given an initial position $\mathbf{s}_0^{1:N_u}$, the optimal cost $J^*(\mathbf{s}_0^{1:N_u})$ is equal to $J_0(\mathbf{s}_0^{1:N_u})$, given by the last step of the following algorithm, which proceeds backward in time from period $N_t - 1$ to 0:

$$J_{N_t}(\mathbf{s}_{N_t}^{1:N_u}) = 0 \tag{31}$$

$$J_k(\mathbf{s}_k^{1:N_u}) = \min_{u_k^{1:N_u} \in U_k^{1:N_u}(\mathbf{s}_k)} \left\{ g_k(\mathbf{s}_k^{1:N_u}, u_k^{1:N_u}) + J_{k+1}(\mathbf{s}_{k+1}^{1:N_u}) \right\} \tag{32}$$

constrained to

$$\begin{cases} \mathbf{s}_{k+1}^v = F(\mathbf{s}_k^v, u_k^v), \quad \mathbf{s}_0^v \qquad v = 1, 2, \cdots, N_u \\ s_k^a \neq \mathbf{s}_k^b, \quad a, b = 1, 2, \cdots, N_u, \quad a \neq b \end{cases} \tag{33}$$

where, $k = N_t - 1, N_t - 2, \cdots, 0$ and

$$g_k(\mathbf{s}_k^{1:N_u}, u_k^{1:N_u}) = \sum_{v=1}^{N_u} \left\{ -I(\boldsymbol{\Theta}^k; \mathbf{z}^k | \mathbf{s}_k^v) + {u_k^v}^T B u_k^v \right\} \tag{34}$$

As mentioned before, this process should be performed for each of the possible values for initial condition $\mathbf{s}_0^v$. After finding the optimal policy U^v, it can then be used to optimally locate the corresponding UAV.

Implementation of above algorithm using the continuous dynamics of the UAV in Eq. (20) requires excessive computational resources and is not achievable in real time. Hence to make the problem tractable, the spatial domain has been discretized into a uniform grid. The mutual information is then only evaluated at these grid nodes and the UAV motion is restricted to these nodes. This lead to a more tractable sub-optimal solution that is implementable in real time. Unfortunately, the problem complexity grows exponentially with the number of UAVs. For instance, even in presence of 2 UAVs and a $100 \times 100 \times 10$ spatial grid points, there will be 10^{10} possible combinations for positions of UAVs for which $J(\mathbf{s}_0^{1:2})$ needs to be minimized. Hence, an enormous computational effort is required to perform such minimization. A simpler alternative approach to overcome these deficiencies in minimizing Eq. (29) is to recursively find *sub-optimal* policies for each one of the UAVs individually with slight modifications

in original cost function. The idea is to first find optimal position for the first UAV during the time. Then, the *sub-optimal* policies for all other UAVs can be found by minimizing the following modified cost function:

$$\min_{U=\{u_0^v, u_1^v, \cdots, u_{N_t-1}^v\}} J(\mathbf{s}_0^v) \tag{35}$$

$$\text{constraint to} = \begin{cases} \mathbf{s}_{k+1}^v = F(\mathbf{s}_k^v, u_k^v) \\ \mathbf{s}_0^v \end{cases} \tag{36}$$

where,

$$J(\mathbf{s}_0^v) = \sum_{k=0}^{N_t-1} \left\{ -I(\boldsymbol{\Theta}_k, \mathbf{z}_k | \mathbf{s}_k^v) + {u_k^v}^T B u_k^v + \alpha \sum_{j=1}^{v-1} e^{-[\mathbf{s}_k^v - \mathbf{s}_k^j]^T W [\mathbf{s}_k^v - \mathbf{s}_k^j]} \right\} \tag{37}$$

where, $v = 2, 3, \cdots, N_u$ and $\alpha > 0$ and the positive definite diagonal matrix W are penalty factors that determine the separation between neighboring UAVs. Hence, the UAVs are made to *spread out* in the spatial domain of interest thus avoiding redundancy in measurements .

One should note that the computational cost involved in recursively finding sub-optimal locations of UAVs is far less than the computational cost involved in solving Eq. (32) to Eq. (34). For comparison, consider a case where N_u UAVs are used to perform data observation over a $N_g \times N_g \times N_g$ spatial grid points. In this case, the computational cost involved in solving Eq. (32) to Eq. (34) will be proportionate to $N_g^{3N_u}$, while the computational cost involved in finding sub-optimal locations of UAVs using Eq. (35) to Eq. (37) is proportionate to $N_u N_g^3$. Hence, solving Eq. (35) results in significantly less computational with respect to solving Eq. (32), especially in presence of larger number of UAVs.

6.3 Limited Lookahead Policy

Depending on the nature of phenomenon under study, evaluation of mutual information map for all the future time steps can be computationally expensive. This will result in computational complexity while finding optimal control policies for the UAVs during source parameter estimation process. Hence, using Eq. (37) restricts real time applications of proposed algorithm. One way to avoid these computational complexities is to approximate the true cost-to-go function J_{k+1} in Eq. (37) with some function, denoted by $\tilde{J}_{k+1}$, which is a *limited lookahead* approximation of true cost-to-go function J_{k+1}. For instance, in Eq. (37), J_{k+1} can be approximated as

$$J_{k+1}(\mathbf{s}_k^v, u_k^v) \simeq \tilde{J}_{k+1}(\mathbf{s}_k^v, u_k^v) =$$
$$\sum_{i=k+1}^{k+1+l} \left\{ -I(\boldsymbol{\Theta}_i, \mathbf{z}_i | F(\mathbf{s}_{i-1}^v, u_{i-1}^v)) + {u_i^v}^T B u_i^v + \alpha \sum_{j=1}^{v-1} e^{-[\mathbf{s}_i^v - \mathbf{s}_i^j]^T W [\mathbf{s}_i^v - \mathbf{s}_i^j]} \right\} \tag{38}$$

where, $v = 2, 3, \cdots, N_u$ and l is the number of future time steps which are used for approximation of true cost-to-go function J_{k+1}. As one can see, evaluation of Eq. (37) requires knowledge of mutual information for all the time steps between $k+1$ and $N_t - 1$. While in *limited lookahead* method, J_{k+1} is approximated by a limited number of future time steps.

Similarly, J_{k+1} in Eq. (32) can be approximated as

$$J_{k+1}(\mathbf{s}_k^v, u_k^v) \simeq \tilde{J}_{k+1}(\mathbf{s}_k^v, u_k^v) = \sum_{i=k+1}^{k+1+l} -I(\boldsymbol{\Theta}_i, \mathbf{z}_i | F(\mathbf{s}_{i-1}^v, u_{i-1}^v)) + {u_i^v}^T B u_i^v, \quad v = 1 \tag{39}$$

Note that when the number of lookahead step is one, i.e. $l = 1$, limited lookahead policy reduces to greedy algorithm which was discussed in Eq. (27) and Eq. (28).

Limited lookahead policy has two major benefits with respect to original Dynamic Programming algorithm. First, as mentioned before, limited lookahead policy could result in considerably less computational cost involved in finding *sub-optimal* control policies. The second benefit of limited lookahead policy is that due to dependence of optimal policies on future wind data, the optimal policies obtained using the original cost function may be erroneous for distant future time steps. Hence, using limited lookahead policy avoids erroneous optimal policies by approximating the true cost-to-go function with limited number of future time steps.

The only drawback of using limited lookahead policy is that it may result in slower convergence of estimation process, especially if the UAVs are located far away from the mutual information map. To illustrate this more clearly, consider the situation shown in Fig. 3. As one can see, if initial position of the UAV is far from mutual information map, given maximum speed of UAV and lookahead time step $l = 3$, there will not be any information in range of the UAV. Hence, the UAV does not move and proposed algorithm suggests that the UAV should stay at the same position during the time.

This shortcome can be overcome by minimizing the distance between the UAV position and mutual information map, whenever the mutual information inside the range of UAV is zero. In this way, the UAV will move toward the mutual information map, even if mutual information map is out of range of UAV in l time step. This can be mathematically described as the following:

If $\sum_{i=k+1}^{k+1+l} I(\boldsymbol{\Theta}_i, \mathbf{z}_i | F(\mathbf{s}_{i-1}^v, u_{i-1}^v)) = 0$, then

$$\tilde{J}_{k+1}(\mathbf{s}_k^v, u_k^v) = \sum_{i=k+1}^{k+1+l} d(\mathbf{s}_{I_{max}}^i, F(\mathbf{s}_{i-1}^v, u_{i-1}^v)), \quad v = 1 \tag{40}$$

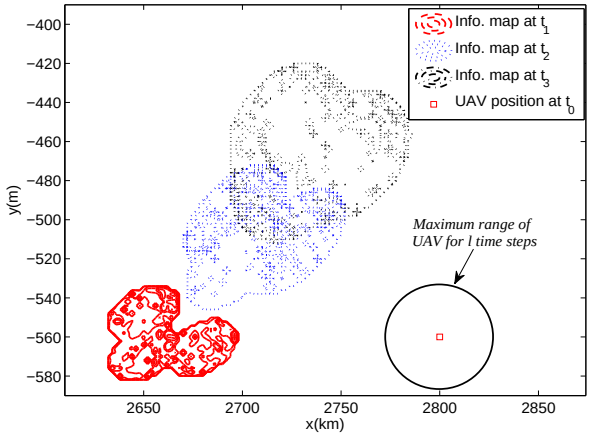

Fig. 3. Schematic layout of applied UAV sensor and mutual information maps at three consecutive times. Red square shows initial position of UAV and black circle shows its maximum range, given maximum speed of UAV and $l = 3$.

and

$$\tilde{J}_{k+1}(\mathbf{s}_k^v, u_k^v) = \sum_{i=k+1}^{k+1+l} d(\mathbf{s}_{I_{max}}^i, F(\mathbf{s}_{i-1}^v, u_{i-1}^v)) + \alpha \sum_{j=1}^{v-1} e^{-[\mathbf{s}_i^v - \mathbf{s}_i^j]^T [\mathbf{s}_i^v - \mathbf{s}_i^j]} \tag{41}$$

where, $v = 2, 3, \cdots, N_u$, and

$$d(\mathbf{s}_{I_{max}}^i, F(\mathbf{s}_{i-1}^v, u_{i-1}^v)) = ||\mathbf{s}_{I_{max}}^i - F(\mathbf{s}_{i-1}^v, u_{i-1}^v)||_2 \tag{42}$$

is the Euclidean distance between the spatial location where mutual information obtains its maximum (denoted by $\mathbf{s}_{I_{max}}^i$) and location of UAV. Using above algorithm, the UAVs always move toward the mutual information map, independent of initial location of UAVs or lookahead time step l. Note that this property of proposed approach warranties faster detection of the plume and consequently faster convergence of estimation process.

7 Numerical Simulations

For numerical simulations, dispersion/advection of propane is simulated over New York area. The domain of interest and the applied wind field (at one specific time) are shown in Fig. 4. Simulation time is considered to be 24 hrs. starting from $00:00$ of September 1^{st}, 2013. North American Regional Reanalysis wind data at pressure level 100 kpa (height $\simeq 100$ m.) is used as the windfield for simulation. Three instantaneous mass releases are considered where their location is known and the only uncertain parameters are their amount of mass release.

It is assumed that releases happen at the same time, i.e. all source releases happen at $00:00$ of September 1^{st}. All mass releases are assumed to be uniformly distributed between 100 kg and 300 kg. Fig. 4 illustrates source locations and the windfield (at $t = 0$ $hrs.$) over the two dimensional spatial domain.

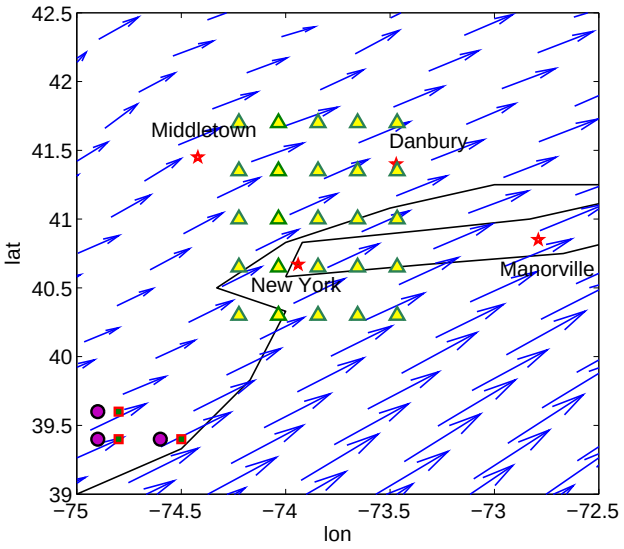

Fig. 4. Schematic layout of Propane release over New York region, source locations are shown with purple circles, the wind-field (at $t = 0$ hr and pressure level = 100 kPa) is shown over the two dimensional domain with blue vector field. Applied networks of stationary sensors are shown with different markers. Green squares show applied 3 stationary sensors, while yellow triangles represent 25 stationary sensors. Geographical location of different cities can be seen on the background map

Plume Dispersion Model

Second-order Closure Integrated PUFF (SCIPUFF) [23] is an atmospheric dispersion model which makes use of Gaussian puff methodology to provide a three-dimensional, time dependent Lagrangian solution to the turbulent diffusion equations. In SCIPUFF model, time-dependent concentration field is represented as a collection of overlapping Gaussian puffs. Each Gaussian puff is described by a total mass, its mean, and measure of the spatial spread (covariance matrix). All the puffs are then transported as Lagrangian elements and their overlap provide overall behavior of a plume due to dispersion/advection.

A key feature of SCIPUFF is the splitting/merging algorithms which improves the representation of inhomogeneous meteorology. In splitting/merging,

puffs are split, conserving all the moments, when they reach a size comparable with the scale of the meteorological grid; similarly, puffs are merged when they grow large enough to overlap their neighbors sufficiently. These techniques are well suited to Lagrangian models, where very large ranges of scales need to be represented. Near the source, puffs may have scales of a few meters or less, but the model is required to calculate effects at ranges up to thousands of kilometers. SCIPUFF has been evaluated using a wide range of field experiments, ranging from the short range CONFLUX experiments with downwind range of several meters up to the ANATEX and ETEX continental scale experiments. For detailed information about SCIPUFF, please refer to [23].

Sensor Model

The sensor used for the measurements is a bar sensor with a discrete numbers of bars similar to the one used in [24], with slight differences. The number of bars ranges from zero to fifteen. These bar readings indicate the concentration magnitude at the sensor location at the instant; the sensor displays $z = 0, \cdots, 15$, bars when the internal continuous-valued concentration magnitude $\mathbf{x}_{int}$ is between thresholds T_z and T_{z+1}, where $0 \leq T_z < T_{z+1}$. The thresholds T_z's are defined on a logarithmic scale, i.e. $T_z \in \{0, 5\times10^{-14}, 10^{-13}, 5\times10^{-13}, 10^{-12}, \cdots, 5\times10^{-7}\}$.

Properties of the sensor are determined by these thresholds and the properties of $\mathbf{x}_{int}$, which is *assumed* to be normally distributed about the true concentration $\mathbf{x}$ [24]. Measurement error $v = \mathbf{x}_{int}$ - $\mathbf{x}$ may be considered a combination of multiplicative noise and additive noise with mean zero and standard deviation $\sqrt{R(\mathbf{x})} = \sigma(\mathbf{x}) = a\mathbf{x} + b$ where a is the proportionality constant and b accounts for the thermal motion of the electrons in the components [24]. In practice, because the true value of $\mathbf{x}$ is never known, $\sigma(\mathbf{x})$ is usually approximated by $\sigma(\tilde{\mathbf{x}})$, where $\tilde{\mathbf{x}}$ is an estimate of $\mathbf{x}$. $a = 1$ and $b = 10^{-15}$ in our simulations. It is also assumed that $\tilde{\mathbf{x}} = T_z$, where T_z is the sensor bar corresponding to $\mathbf{x}_{int}$. Probability density function of $\mathbf{x}_{int}$ given the corresponding concentration $\mathbf{x}$ is

$$p(\mathbf{x}_{int}|\mathbf{x}) = \mathcal{N}(\mathbf{x}_{int}; \mathbf{x}, R) = \frac{1}{\sqrt{2\pi R}} e^{-\frac{(\mathbf{x}_{int}-\mathbf{x})^2}{2R}} \tag{43}$$

where, $\mathcal{N}(,;.,.)$ denotes a Gaussian probability density function with the mean and variance specified by its second and third arguments. Strictly speaking, $p(\mathbf{x}_{int}|\mathbf{x})$ is not a Gaussian distribution because it is only defined for non-negative values of $\mathbf{x}_{int}$. Following Eq. (43), likelihood function, or simply probability of $\mathbf{z}$ conditioned on $\mathbf{x}$, is determined by the following integral

$$P(\mathbf{z}|\mathbf{x}) \propto \int_{T_z}^{T_{z+1}} p(\mathbf{x}_{int}|\mathbf{x}) d\mathbf{x}_{int}, \quad \sum_z P(\mathbf{z}|\mathbf{x}) = 1 \tag{44}$$

Note that due to discretization involved in sensor output, the mutual information in Eq. (18) will be written as

$$I(\boldsymbol{\Theta};\mathbf{z}) = \sum_{z=0}^{N_z}\sum_{q=1}^{M} w_q \Gamma(T_{z+1}, T_z, \boldsymbol{\Theta}(\boldsymbol{\xi}^q), R) \ln\left(\Gamma(T_{z+1}, T_z, \boldsymbol{\Theta}(\boldsymbol{\xi}^q), R)\right) - \sum_{z=0}^{N_z}\left(\sum_{q=1}^{M} w_q \Gamma(T_{z+1}, T_z, \boldsymbol{\Theta}(\boldsymbol{\xi}^q), R)\right) \ln\left(\sum_{q=1}^{M} w_q \Gamma(T_{z+1}, T_z, \boldsymbol{\Theta}(\boldsymbol{\xi}^q), R)\right)$$

where,

$$\Gamma(T_{z+1}, T_z, \boldsymbol{\Theta}(\boldsymbol{\xi}^q), R) = \frac{1}{2}\left\{\text{erf}\left(\frac{T_{z+1} - \mathbf{x}(\boldsymbol{\Theta})}{\sqrt{2R}}\right) - \text{erf}\left(\frac{T_z - \mathbf{x}(\boldsymbol{\Theta})}{\sqrt{2R}}\right)\right\}$$

and $N_z = 15$. Note that quadrature scheme is used to evaluate the integrals in $I(\boldsymbol{\Theta};\mathbf{z})$.

A set of 59 CUT8 quadrature points are used to quantify the uncertainty involved in concentration of dispersal material. Also, a 6^{th} order gPC expansion is used to reconstruct distribution of parameters after each update. Simulation of dispersion/advection has been performed using SCIPUFF numerical model, where concentration of propane is recorded every 10 $mins$.

Performance of DDM approach is verified by comparing data assimilation results obtained by mobile and stationary sensors. Three sensors are used for data observation and a limited lookahead policy with $l = 6$ is used for finding location of each mobile sensor during the time. We considered $\alpha = 5$ and $W = diag([1, 1])$ in our simulation. Fig. 5(a) illustrates positions of UAVs during the time over the spatial domain. It can be observed from Fig. 5(a) that the UAVs follow the plume during the time and end up to the locations where the mutual information map obtains its maximum.

Convergence behavior for mean estimate of source parameters m_2 and m_3 using stationary sensors, along the minimum and maximum range of estimation are shown in Fig. 6. Fig. 6 illustrates that using stationary sensors results in poor estimates of the parameters. This is due to the inefficient placement of sensors during data assimilation process.

Fig. 7 illustrates convergence behavior for mean estimate of source parameters m_1 and m_2 using mobile sensors. As Fig. 7 represents, DDM approach results in significantly better convergence for mean estimates of the parameters. In addition, estimation process is very confident about the source parameters estimates.

Table 1 shows the amount of information $I(\boldsymbol{\Theta};\mathbf{z})$ collected by each sensor while using stationary and mobile sensors. It is clear from Table 1 that using Dynamic Data Monitoring method significantly increases the amount of mutual information collected by each sensor during the data assimilation process, and consequently improves the convergence behavior of the estimation process.

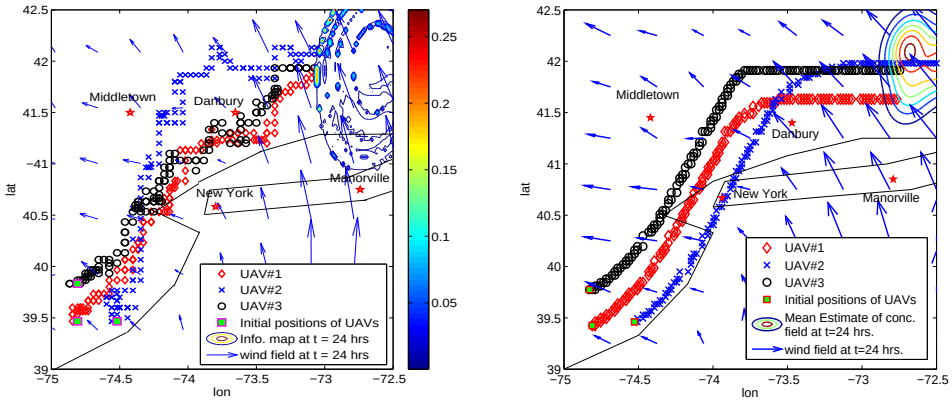

(a) (b)

Fig. 5. a) Obtained way-points for mobile sensors at different time steps based on maximizing mutual information content. Contour map and corresponding colorbar represent the information map at the final time. b) Obtained way-points for mobile sensors at different time steps using Chemotaxis strategy. Contour map represents the mean estimate of concentration field at the final time. The windfield at $t = 24\ hr$ (pressure level $=$ 100 kpa) and geographical map of the region are shown in the background.

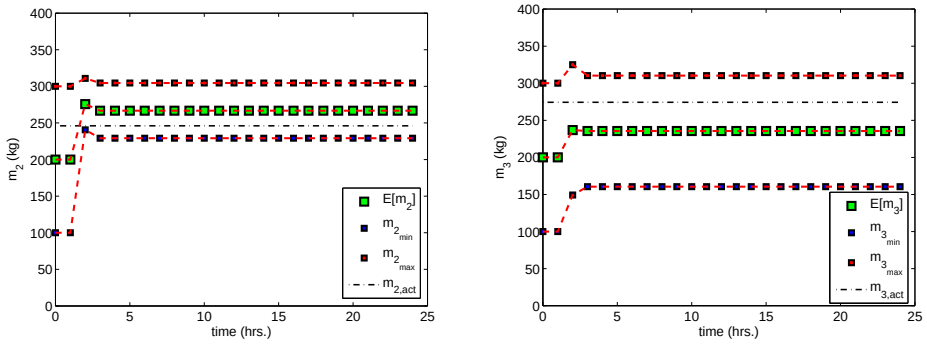

(a) (b)

Fig. 6. Source parameter estimates during the time obtained using stationary sensors

To further illustrate performance of proposed methodology, we have utilized chemotaxis strategy (i.e. moving UAVs along gradient of concentration field) to estimate uncertain source parameters. The same structure for mobile sensors is used while implementing chemotaxis strategy. Obtained way-points for mobile sensors while using chemotaxis strategy can be seen in Fig. 5(b). Fig. 8 illustrate convergence for mean estimate of source parameters m_1 and m_2 using chemotaxis algorithm. As expected, using chemotaxis method results in better convergence comparing with stationary sensors, but its performance is not as good as DDM

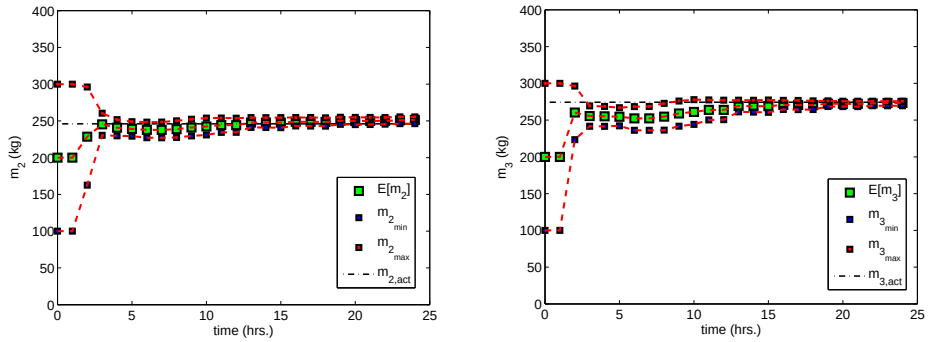

Fig. 7. Source parameter estimates during the time, obtained using DDM method

Table 1. Information collected by each sensor while with and without using Dynamic Data Monitoring approach.

sensor number	collected information	
	Stationary	Dynamic
sensor 1	1.8743	8.2208
sensor 2	1.4219	6.8420
sensor 3	1.4009	7.1927

approach and obtained estimates for source parameters are not as confident as those of DDM method.

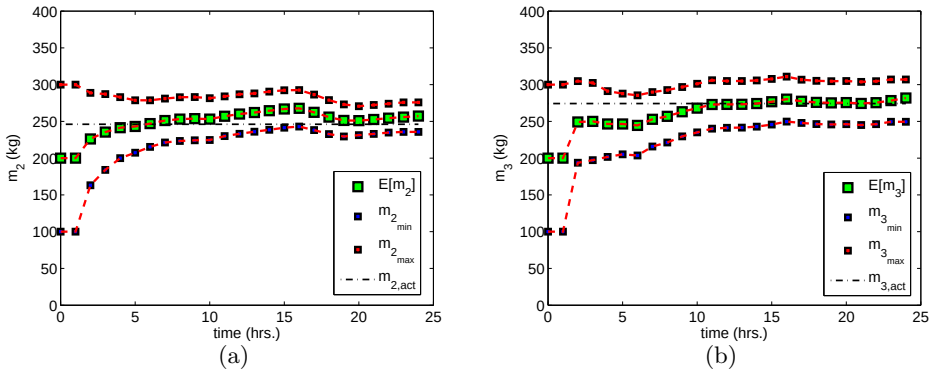

Fig. 8. Source parameter estimates during the time, obtained using Chemotaxis method

To summarize, Root Mean Square Error (RMSE) between mean estimate of source parameters and their actual values while using different sensor networks and different methods is shown in Table 2. It is clear from Table 2 that proposed DDM algorithm outperforms all the other alternative methods or sensor networks, and DDM approach results in least amount of RMSE comparing to other sensor networks and chemotaxis algorithm. To highlight performance of proposed DDM approach, we have also compared RMSE in parameter estimates obtained by DDM approach with RMSE of source parameter estimates using 25 stationary sensors (shown with blue crosses in Fig. 4). As Table 2 represents, using DDM approach with just 3 sensors results in lower value of RMSE in parameter estimates, comparing with 25 stationary sensors. Hence, proposed DDM method provides more accurate estimates while using less number of data observation sensors at the same time.

Table 2. Root Mean Square Error (RMSE) between mean estimate of source parameters and their actual values while using different sensor networks and different methods.

sensor network/method	RMSE		
	m_1	m_2	m_3
3 *stationary* sensors	46.27	21.18	38.67
25 *stationary* sensors	14.49	19.42	33.86
3 *mobile* sensors / chemotaxis	16.11	11.97	14.32
3 *mobile* sensors / DDM	1.93	5.74	12.19

8 Conclusion

In this research, an end-to-end method was developed to estimate the source parameters of a dispersion phenomenon using optimally placed data monitoring sensors. The key idea of the presented method is to optimally locate data monitoring sensors such that the mutual information between model predictions and data measurements is maximized thereby giving a better reduction in uncertainty. The main advantage of this approach is that it *significantly increases* the accuracy of the estimation algorithm, while using *fewer* number of data observation sensors. Further, a new set of quadrature points, known as CUT, are used to alleviate the computational complexity involved in the propagation of uncertainty in the parameters. The limited lookahead dynamic programming approach is well suited for the current problem as it is capable of incorporating or assimilating the updated information of wind data and measurements and thus provides robust UAV trajectories to collect better measurements. Mutual collisions and measurement redundancy are avoided by constantly maintaining

a sufficient separation between UAVs at all times. The numerical simulations validate the proposed methodology where the mobile sensors, when optimally planned to make measurements at specific locations and specific time instances, provide better estimates that significantly outperform the estimates from stationary sensors. It is emphasized that the proposed dynamic data monitoring method can be applied to other types of data assimilation problems, especially in large scale systems with Hidden Markov Models or even black-box models with minor modifications.

9 Acknowledgement

This material is based upon work supported by the National Science Foundation under award number CMMI- 1054759 and AFOSR grant number FA9550-11-1-0012.

References

1. X. Zheng, Z. Chen, Inverse calculation approaches for source determination in hazardous chemical releases, Journal of Loss Prevention in the Process Industries 24 (4) (2011) 293–301. doi:10.1016/j.jlp.2011.01.002.
2. K. Shankar Rao, Source estimation methods for atmospheric dispersion, Atmospheric Environment 41 (33) (2007) 6964–6973.
3. G. Sandini, G. Lucarini, M. Varoli, Gradient driven self-organizing systems, in: Intelligent Robots and Systems' 93, IROS'93. Proceedings of the 1993 IEEE/RSJ International Conference on, Vol. 1, IEEE, 1993, pp. 429–432.
4. A. T. Hayes, A. Martinoli, R. M. Goodman, Swarm robotic odor localization, in: Intelligent Robots and Systems, 2001. Proceedings. 2001 IEEE/RSJ International Conference on, Vol. 2, IEEE, 2001, pp. 1073–1078.
5. D. Zarzhitsky, D. F. Spears, W. M. Spears, Distributed robotics approach to chemical plume tracing, in: Intelligent Robots and Systems, 2005.(IROS 2005). 2005 IEEE/RSJ International Conference on, IEEE, 2005, pp. 4034–4039.
6. H.-L. Choi, J. P. How, Continuous trajectory planning of mobile sensors for informative forecasting, Automatica 46 (8) (2010) 1266–1275.
7. F. Bourgault, A. A. Makarenko, S. B. Williams, B. Grocholsky, H. F. Durrant-Whyte, Information based adaptive robotic exploration, in: Intelligent Robots and Systems, 2002. IEEE/RSJ International Conference on, Vol. 1, IEEE, 2002, pp. 540–545.
8. B. J. Julian, M. Angermann, M. Schwager, D. Rus, Distributed robotic sensor networks: An information-theoretic approach, The International Journal of Robotics Research 31 (10) (2012) 1134–1154.
9. S. MartíNez, F. Bullo, Optimal sensor placement and motion coordination for target tracking, Automatica 42 (4) (2006) 661–668.
10. R. Tharmarasa, T. Kirubarajan, M. L. Hernandez, Large-scale optimal sensor array management for multitarget tracking, Systems, Man, and Cybernetics, Part C: Applications and Reviews, IEEE Transactions on 37 (5) (2007) 803–814.
11. J. L. Williams, J. W. Fisher, A. S. Willsky, Approximate dynamic programming for communication-constrained sensor network management, Signal Processing, IEEE Transactions on 55 (8) (2007) 4300–4311.

12. G. M. Hoffmann, C. J. Tomlin, Mobile sensor network control using mutual information methods and particle filters, Automatic Control, IEEE Transactions on 55 (1) (2010) 32–47.
13. N. Adurthi, The conjugate unscented transform - a method to evaluate multidimensional expectation integrals, Master's thesis, University at Buffalo.
14. A. Nagavenkat, P. Singla, T. Singh, The conjugate unscented transform-an approach to evaluate multi-dimensional expectation integrals, Proceedings of the American Control Conference, 2012.
15. A. Nagavenkat, P. Singla, T. Singh, Conjugate unscented transform rules for uniform probability density functions, Proceedings of the American Control Conference, 2013.
16. A. Nagavenkat, P. Singla, T. Singh, Conjugate unscented transform and its application to filtering and stochastic integral calculation, AIAA Guidance, Navigation, and Control Conference, 2012.
17. R. Bellman, R. Kalaba, Selected Papers on Mathematical Trends in Control Theory, Dover, New York, NY, 1964.
18. D. P. Bertsekas, Dynamic Programming and Optimal Control, vols I and II, Cambridge, 2000.
19. R. Madankan, P. Singla, T. Singh, P. Scott, Polynomial chaos based bayesian approach for state and parameter estimation, AIAA Journal of Guidance, Navigation, and Control, In Press.
20. N. Wiener, The Homogeneous Chaos, American Journal of Mathematics 60 (4) (1938) 897–936.
21. D. Xiu, G. E. Karniadakis, The Wiener–Askey Polynomial Chaos for Stochastic Differential Equations, SIAM J. Sci. Comput. 24 (2) (2002) 619–644. doi:http://dx.doi.org/10.1137/S1064827501387826.
22. T. M. Cover, J. A. Thomas, Elements of Information Theory (Wiley Series in Telecommunications and Signal Processing), Wiley-Interscience, 2006.
23. R. I. Sykes, S. F. Parker, D. S. Henn, SCIPUFF Version 2.2 Technical Documentation (729).
24. P. Robins, V. Rapley, P. Thomas, A probabilistic chemical sensor model for data fusion, in: Information Fusion, 2005 8th International Conference on, Vol. 2, IEEE, 2005, pp. 7–pp.